DNA Nanostructures

DOI: 10.1002/anie.201108710

DNA-Directed Three-Dimensional Protein Organization**

*Chuan Zhang, Cheng Tian, Fei Guo, Zheng Liu, Wen Jiang, and Chengde Mao**

Three-dimensional (3D) self-assembly is a basic process in nature. Often multiple components cooperatively assemble together to form functional biological devices, for example, viruses and organelles in the cell. Despite extensive efforts to mimic such a process for the preparation of artificial nanodevices, it remains a grand challenge. Various types of materials have been used to study the molecular 3D self-assembly process. Among them, DNA stands as an excellent candidate[1] and a range of DNA 3D nanostructures have been successfully programmed to self-assemble.[2–12] However, the complexity of such structures is low. One rational approach to increase their complexity and introduce functionality is to decorate such DNA 3D nanostructures with other molecular components, such as proteins.[4,13,14] Herein, we report an exploration in this direction by assembly of DNA–protein chimerical 3D nanostructures.

DNA–protein chimerical 3D complexes self-assemble in two steps (Figure 1): 1) programmed self-assembly of symmetric DNA polyhedra followed by 2) immobilization of proteins onto the DNA scaffolds. Recently a family of star-shaped, symmetric DNA nanomotifs has been developed.[15–16] Each motif is assembled from three different types of DNA strands: a long, repetitive strand (Ln; n = 3–5; blue and red); medium strands (M; green); and short, peripheral strands (S; black). All DNA motifs share the same M and S strands, but use different L strands, which contain different numbers (n) of sequence repeats. The motifs have been programmed to assemble into symmetric polyhedra in a process similar to the self-assembly of viral capsids. To immobilize protein streptavidin (STV) onto the DNA polyhedra, we have incorporated a biotin moiety at the 5′ end of strand S so we can take advantage of the specific and strong interaction between biotin and STV. Upon DNA self-assembly, each face of the DNA polyhedra displays three biotin moieties, which are related by a three-fold rotational symmetry (Figure 1, lower right). When these polyhedra are incubated with STV, each DNA polyhedral face can bind to STV at three biotin binding sites (each STV protein has four biotin binding sites). The trivalent binding is not only much stronger than the binding of one biotin to STV, but more importantly, also greatly reduces the freedom of the bound STV relative to the DNA scaffolds. Controlling the guest freedom is a great challenge for DNA-directed guest organization and has rarely been experimentally addressed in the literature.[17]

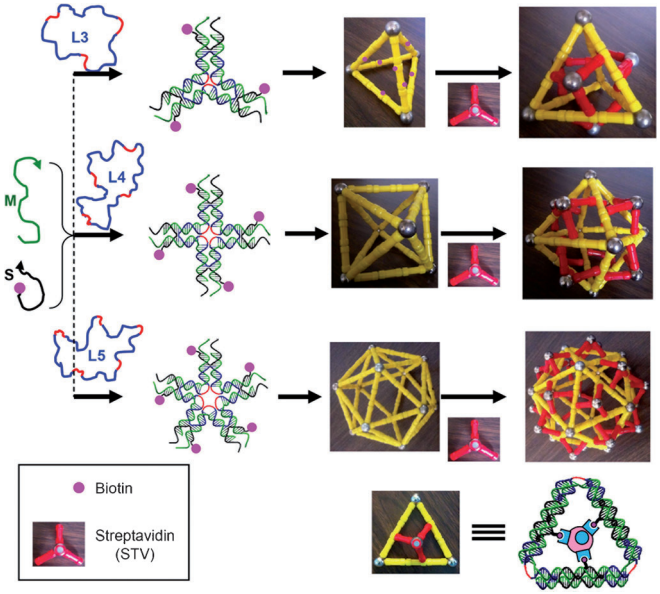

Figure 1. Schematic representation of the 3D protein organization directed by DNA nanostructures. DNA strands L (blue and red), M (green), and S (black; conjugated to a biotin at its 5′ end) self-assemble, by maximizing the base pairing between complementary DNA segments, into star-shaped nanomotifs that further assemble into symmetric DNA polyhedra: tetrahedron (TET), octahedron (OCT), and icosahedron (ICO). Each vertex is composed of a corresponding DNA star-shaped motif. All faces of the DNA polyhedra are identical triangles and display three biotin moieties. Upon incubation with streptavidin (STV) protein, each polyhedral face will bind to a STV protein, thus resulting in well-structured TET/STV, OCT/STV, and ICO/STV complexes. The lower right-hand section shows the details of the trivalent binding between a STV protein and a triangular face of the DNA polyhedra. Note that the plastic rods/metal balls are used as a convenient and intuitive model instead of a precise structural model.

We started our investigation with the organization of STV onto a DNA tetrahedron (Figure 1 and 2), because the tetrahedron is the simplest DNA polyhedron. Reported protocols were followed for the assembly process.[3,4] A brief explanation of the assembly process is as follows: the corresponding DNA strands (L_3/M/S = 1:3:3) were mixed in a Mg^{2+} containing, neutral, aqueous buffer and slowly cooled down from 95 °C to 25 °C over 48 hours, and then incubated

[*] C. Zhang, C. Tian, Prof. C. Mao
Department of Chemistry, Purdue University
560 Oval Dr., West Lafayette, IN 47907 (USA)
E-mail: mao@purdue.edu
F. Guo, Z. Liu, Prof. W. Jiang
Department of Biological Sciences and Markey Center of Structural Biology, Purdue University
560 Oval Dr., West Lafayette, IN 47907 (USA)

[**] We thank the Office of Naval Research and the National Science Foundation for supporting this research. AFM and DLS studies were carried out in the Purdue Laboratory for Chemical Nanotechnology (PLCN). The cryo-EM images were taken in the Purdue Biological Electron Microscopy Facility and the Purdue Rosen Center for Advanced Computing (RCAC) provided the computational resource for the 3D reconstructions.

Supporting information for this article is available on the WWW under http://dx.doi.org/10.1002/anie.201108710.

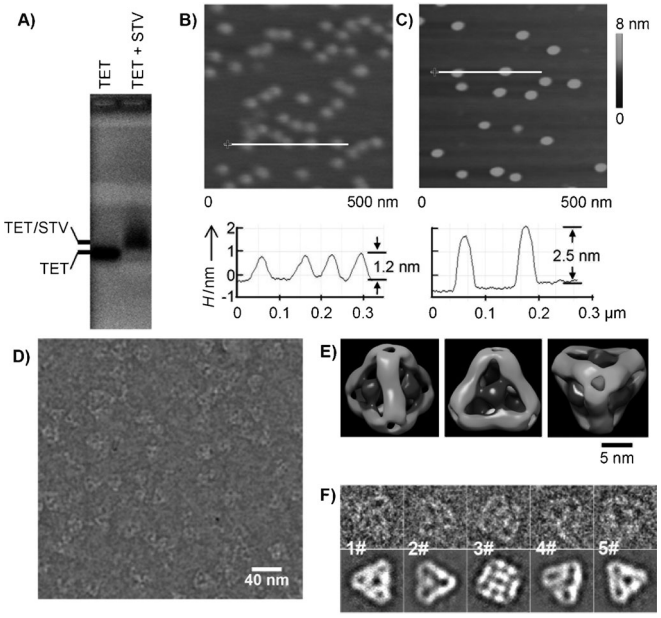

Figure 2. Experimental characterization of the TET/STV complex. A) Agarose-gel electrophoretic analysis of the TET/STV binding. B) and C) Atomic force microscopy (AFM) images of unbound TET and the TET/STV complex, respectively. Below the images are the height profiles along the lines shown in the images. D) A cryogenic electron microscopy (cryoEM) image of the TET/STV complex. E) Three views of the TET/STV complex structure that is reconstructed from the cryoEM images of the sample. F) Comparison between the raw cryoEM images (top) and the 2D projections (bottom) of the reconstructed, structural model.

with STV at 25 °C for approximately 16 hours. After assembly, we first confirmed the binding of STV by 1 % agarose gel electrophoresis under a native condition (Figure 2 A). Clearly, STV binds to the DNA tetrahedron (TET) and causes an electrophoretic mobility shift. Although an STV protein has four biotin binding sites, neither crosslinking between TETs nor large aggregates were observed, thus indicating that each STV binds to only one TET. We attribute this phenomenon to the cooperative, trivalent interaction between STV and each TET face (bearing three biotin moieties; see scheme at lower right in Figure 1). The trivalent binding mode is supported by a partial denaturation experiment (see the Supporting Information, Figure S1).[18] After assembly, the TET/STV complex was denatured under mild denaturing conditions, such that the DNA duplexes were completely dissociated into single strands but most of the strong biotin–STV interactions were unaffected. Then the partially denatured mixture was analyzed by polyacrylamide gel electrophoresis (PAGE) under the same denaturing conditions. From the gel, it is evident that one STV protein binds to three biotinylated DNA strands and no single STV protein binds to four biotinylated DNA strands, a result which is consistent with the designed trivalent binding mode.

Microscopy imaging allows the direct visualization of the TET/STV complex. Atomic-force microscopy (AFM) imaging shows that TET/STV complex is significantly taller than TET itself (Figure 2 B and C). The absolute height values are not accurate, because of dehydration and strong interactions between the sample and substrate, but the relative height change is consistent with the expected value. The AFM imaging also confirms that the TET/STV complex particles are quite uniform in size and no crosslinking between TETs happens. We have further characterized the TET/STV complex by cryogenic electron microscopy (cryoEM). A very thin layer of TET/STV solution was flash frozen, which is believed to keep the DNA/STV complex in its native conformation and allow visualization of the protein arrangement in 3D. In the raw cryoEM images (Figure 2 D), most visible particles have a tetrahedral shape and are of the expected size. The observed edges are 14 nm long, thus matching the designed model (13.8 nm), if it is assumed that a DNA duplex has a pitch of 0.33 nm per base pair and a diameter of 2 nm. For the experimentally observed particles, the structure of the TET/STV complex (Figure 2 E) at a resolution of 2.9 nm was revealed by single particle 3D reconstruction, a well-developed technique used in structural biology.[19,20] 2D projections computed from this structural model match with the individual, raw-particle images (Figure 2 F) and the class averages of raw particles with similar orientations (Figure S2). In the reconstructed structural model, extra density exists at the center of each TET face and corresponds to STV protein. It is also clear that each STV protein binds to one TET face through three binding sites. Such a structural feature is consistent with our design.

STV is not passively organized by the DNA scaffold, but actively impacts on the DNA scaffold. At least two phenomena emerge upon STV binding. First, STV binding causes distortion to the DNA struts in TET (Figure 2 E and Figure S3). The DNA struts are straight rods in the unbound TET,[15] but become bent in the DNA/STV complex. We speculate that it is because of the subtle distance mismatch between the biotins displayed by the TET and the biotin binding sites of the STV protein. Because of the strong biotin–STV interaction, TET becomes slightly deformed during the binding of STV to allow binding of the STV to the biotin. It remains to be tested whether such a guest-induced structural change is a general phenomenon in DNA-directed guest organization. Second, binding of the STV increases the TET stability. For the unbound TET, the DNA motifs are held together solely by DNA hybridization. In contrast, for the TET/STV complex, the DNA motifs are held together by both DNA hybridization and the binding between the STV and biotin. Hence, the TET/STV complex is expected to be more stable than the unbound TET. To test this hypothesis, we performed a thermal denaturation experiment by monitoring the hydrodynamic radius (R_H) of both TET and the TET/STV complex with dynamic light scattering (DLS) at different temperatures (Figure 3). When the temperature is increased to a certain value, the complexes will dissociate and the R_H of the particle will dramatically decrease. This temperature is the melting temperature (T_m) of the complex. The DLS study shows that the T_m for the TET/STV complex is approximately 5 °C higher than that of TET itself, thus confirming that TET/STV is indeed more stable than TET itself.

The strategy of organizing proteins by self-assembled DNA polyhedra is a general strategy. In addition to using TET as the scaffold to organize STV, we have demonstrated

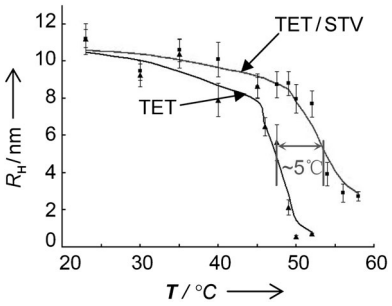

Figure 3. Thermal stability of the TET and TET/STV complex. The hydrodynamic radius (R_H) is monitored by dynamic light scattering (DLS). Each point is an average of five repeated measurements and the standard deviation is indicated by a vertical bar.

that other discrete DNA 3D structures (OCT and ICO) can equally serve as scaffolds to organize STV into structurally well-defined, discrete 3D assemblies (Figures 4 and 5).

This strategy can also be extended beyond STV to other proteins as long as specific interactions can be engineered between the protein and the DNA scaffolds. To demonstrate this application, we have used TET to organize antibody (Ab) protein. Antibodies are a huge family of proteins involved in the immune system. To immobilize antibodies onto TET, the biotin moiety is replaced by a specific antigen (here we used fluorescein as the antigen) at the 5′ end of the S strand. Upon DNA self-assembly, TET displays antigen (fluorescein) instead of biotin. Through strong and specific antibody–antigen interactions, the anti-fluorescein antibody (IgG; MW

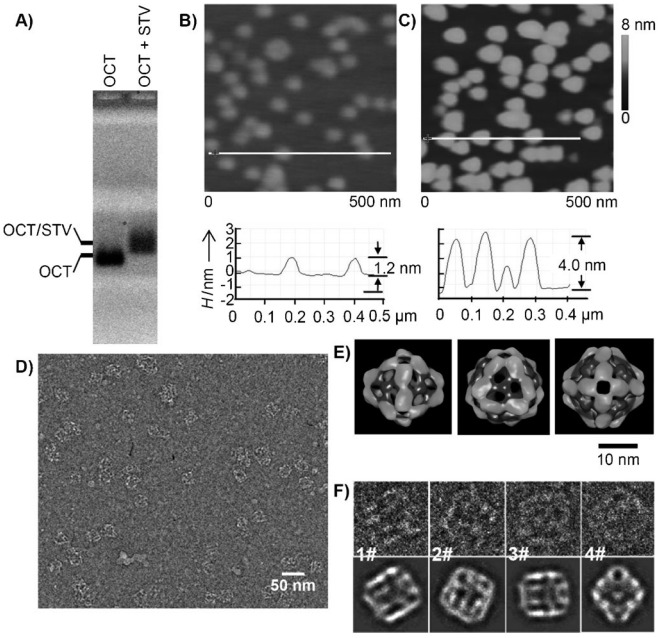

Figure 4. OCT/STV complex. A) Electrophoretic analysis. AFM images of unbound OCT (B) and OCT/STV complex (C). D) A cryoEM image of a sample of the OCT/STV complex. E) Three views of the reconstructed structural model. F) Comparison between the raw cryoEM images (top) and the 2D projections (bottom) of the reconstructed, structural model.

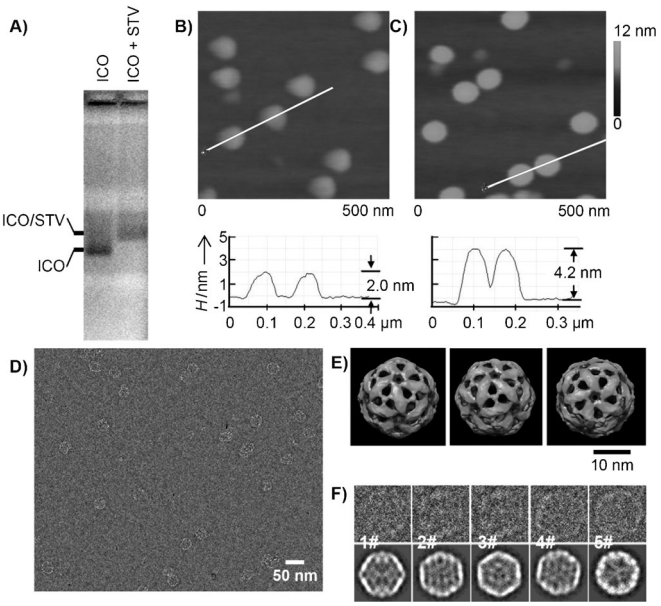

Figure 5. ICO/STV complex. A) Electrophoretic analysis. AFM images of unbound CO (B) and ICO/STV complex (C). D) A cryoEM image of the ICO/STV complex sample. E) Three views of the reconstructed structural model. F) Comparison between the raw cryoEM images (top) and the 2D projections (bottom) of the reconstructed, structural model.

≈150 kD) can specifically bind to fluorescein. The fluorescein 3D distribution will determine the antibody 3D organization. Figure 6 provides experimental proof that antibodies are organized onto the TET. Because of the steric hindrance, an antibody will not simultaneously bind to two fluorescein moieties on one DNA strut. Instead, it will bind to two fluorescein moieties displayed on one triangular face. Note that an antibody can have three different binding modes in each trianglular face (Figure S7). During single-particle reconstruction, the final density map is the average of more than one thousand particles and a threefold rotational symmetry is applied to each triangular face (the symmetry is imposed for quick convergence). Thus in the reconstructed structure, each triangle is an average of the three different binding modes. The average introduces an artifact to the individual protein structure. However, it does not affect the overall antibody arrangement in the TET/Ab complex and, clearly, the antifluorecein antibody is well organized by the TET scaffold.

In summary, we have developed a strategy to use self-assembled DNA nanostructures to organize proteins in 3D space for the preparation of symmetric, discrete 3D protein assemblies. Such structurally well-defined, multicomponent, protein-containing structures can not be systematically prepared by other means. This strategy can be applied to different 3D DNA nanostructures and different proteins. It is conceivable that if aptamers[21] (which are short strands of nucleic acids and can strongly bind to specific ligands) are introduced, the DNA scaffolds could organize an even wider range of objects. The DNA/protein complexes shown in this study superficially resemble many virus structures. Both contain nucleic acids and multiple copies of a few protein

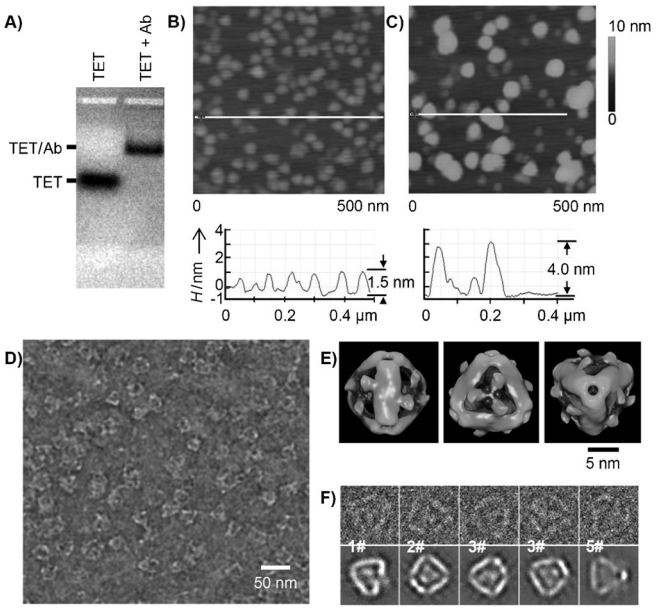

Figure 6. TET/antibody (Ab) complex. A) Electrophoretic analysis. AFM images of unbound TET (B) and TET/Ab complex (C). D) A cryoEM image of the TET/Ab complex sample. E) Three views of the reconstructed structural model of the TET/Ab complex. F) Comparison between the raw cryoEM images (top) and the 2D projections (bottom) of the reconstructed, structural model.

components and are highly symmetric. We believe that our engineered DNA/protein binary structures would provide a platform for biophysical study of viruses such as their self-assembly, stability, mechanic properties, and biological multivalent interactions. It is also possible to use such nanostructures as multivalent vaccines as they resemble virus structures and display multiple copies of identical proteins (potential antigens). We believe that these nanostructures will induce much stronger immune responses than individual protein antigens.

Received: December 10, 2011
Published online: February 28, 2012

Keywords: DNA · nanostructures · proteins · self-assembly · supramolecular chemistry

[1] N. C. Seeman, *Annu. Rev. Biochem.* **2010**, *79*, 65.
[2] J. H. Chen, N. C. Seeman, *Nature* **1991**, *350*, 631.
[3] E. Winfree, F. R. Liu, L. A. Wenzler, N. C. Seeman, *Nature* **1998**, *394*, 539.
[4] H. Yan, S. H. Park, G. Finkelstein, J. H. Reif, T. H. LaBean, *Science* **2003**, *301*, 1882.
[5] P. W. K. Rothemund, N. Papadakis, E. Winfree, *PLoS Biol.* **2004**, *2*, 2041.
[6] W. M. Shih, J. D. Quispe, G. F. Joyce, *Nature* **2004**, *427*, 618.
[7] P. W. K. Rothemund, *Nature* **2006**, *440*, 297.
[8] R. P. Goodman, I. A. T. Schaap, C. F. Tardin, C. M. Erben, R. M. Berry, C. F. Schmidt, A. J. Turberfield, *Science* **2005**, *310*, 1661.
[9] S. M. Douglas, H. Dietz, T. Liedl, B. Hogberg, F. Graf, W. M. Shih, *Nature* **2009**, *459*, 414.
[10] H. Dietz, S. M. Douglas, W. M. Shih, *Science* **2009**, *325*, 725.
[11] E. S. Andersen et al., *Nature* **2009**, *459*, 73.
[12] W. Liu, H. Zhong, R. Wang, N. C. Seeman, *Angew. Chem.* **2011**, *123*, 278; *Angew. Chem. Int. Ed.* **2011**, *50*, 264.
[13] a) N. Wong, C. Zhang, L. Tan, Y. Lu, *Small* **2011**, *7*, 1427; b) C. M. Erben, R. P. Goodman, A. J. Turberfield, *Angew. Chem.* **2006**, *118*, 7574; *Angew. Chem. Int. Ed.* **2006**, *45*, 7414; c) B. P. Duckworth, Y. Chen, J. W. Wollack, Y. Sham, J. D. Mueller, T. A. Taton, M. D. Distefano, *Angew. Chem.* **2007**, *119*, 8975; *Angew. Chem. Int. Ed.* **2007**, *46*, 8819; d) C. M. Niemeyer, *Angew. Chem.* **2010**, *122*, 1220; *Angew. Chem. Int. Ed.* **2010**, *49*, 1200.
[14] J. Sharma, R. Chhabra, R. A. Cheng, J. Brownell, Y. Liu, H. Yan, *Science* **2009**, *323*, 112.
[15] Y. He, T. Ye, M. Su, C. Zhang, A. E. Ribbe, W. Jiang, C. Mao, *Nature* **2008**, *452*, 198.
[16] a) C. Zhang, M. Su, Y. He, X. Zhao, P. Fang, A. E. Ribbe, W. Jiang, C. Mao, *Proc. Natl. Acad. Sci. USA* **2008**, *105*, 10665; b) Y. He, M. Su, P. Fang, C. Zhang, A. E. Ribbe, W. Jiang, C. Mao, *Angew. Chem.* **2010**, *122*, 760; *Angew. Chem. Int. Ed.* **2010**, *49*, 748.
[17] a) Y. He, Y. Tian, A. E. Ribbe, C. Mao, *J. Am. Chem. Soc.* **2006**, *128*, 12664; b) A. Kuzuya, K. Numajiri, M. Komiyama, *Angew. Chem.* **2008**, *120*, 3448; *Angew. Chem. Int. Ed.* **2008**, *47*, 3400; c) K. Numajiri, T. Yamazaki, M. Kimura, A. Kuzuya, M. Komiyama, *J. Am. Chem. Soc.* **2010**, *132*, 9937.
[18] K. Numajiri, A. Kuzuya, M. Komiyama, *Bioconjugate Chem.* **2010**, *21*, 338.
[19] S. J. Ludtke, P. R. Baldwin, W. Chiu, *J. Struct. Biol.* **1999**, *128*, 82.
[20] T. D. Goddard, C. C. Huang, T. E. Ferrin, *J. Struct. Biol.* **2007**, *157*, 281.
[21] E. J. Cho, J. W. Lee, A. D. Ellington, *Annu. Rev. Anal. Chem.* **2009**, *2*, 241.

